Article

In Situ Spectroscopic Study of the Oxidation and Reduction of Pd(111)

Guido Ketteler, D. Frank Ogletree, Hendrik Bluhm, Hongjian Liu, Eleonore L. D. Hebenstreit, and Miquel Salmeron

J. Am. Chem. Soc., **2005**, 127 (51), 18269-18273• DOI: 10.1021/ja055754y • Publication Date (Web): 02 December 2005

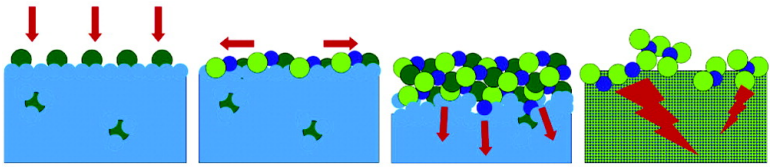

J|A|C|S
ARTICLES
Published on Web 12/02/2005

In Situ Spectroscopic Study of the Oxidation and Reduction of Pd(111)

Guido Ketteler,* D. Frank Ogletree, Hendrik Bluhm,† Hongjian Liu, Eleonore L. D. Hebenstreit, and Miquel Salmeron

Contribution from the Lawrence Berkeley National Laboratories, Materials Sciences Division, University of California, Berkeley, California 94720

Received August 22, 2005; E-mail: gketteler@lbl.gov

Abstract: Using a photoemission spectroscometer that operates close to ambient conditions of pressure and temperature we have determined the Pd−O phase diagram and the kinetic parameters of phase transformations. We found that on the (111) surface oxidation proceeds by formation of stable and metastable structures. As the chemical potential of O_2 increases chemisorbed oxygen forms followed by a thin surface oxide. Bulk oxidation is a two-step process that starts with the metastable growth of the surface oxide into the bulk, followed by a first-order transformation to PdO.

Introduction

Despite their importance the atomic scale processes leading to the oxidation of metals are not understood. This is in part due to the lack of techniques that provide information about the metal-oxide equilibrium structure and kinetics in situ. Techniques that can differentiate between different oxidation states, such as electron spectroscopy, cannot operate under the O_2 pressures and temperature relevant to the oxidation process, typically near atmospheric pressure. The oxidation of metals proceeds by chemisorption of oxygen, surface oxidation, oxygen incorporation to the subsurface region, and bulk oxidation.[1−11] Chemisorption and surface oxidation have been studied by surface sensitive techniques in ultrahigh vacuum, but not much is known about subsurface incorporation and bulk oxidation of late transition metals. Buildup of oxygen in the subsurface region seems to be crucial for several complex phenomena that have been described on platinum group metal surfaces in the presence of oxygen, such as oscillations in reaction rate during CO oxidation,[12] and hysteresis in oxidation−reduction cycles.[13,14] Oxidized Palladium has been suggested to be an active catalyst for the removal of hydrocarbons and CO in car exhaust converters[15] and in the combustion of methane.[16]

Studies of oxygen incorporation in the subsurface during oxidation of late transition metals have been performed by quenching Ru(0001) and Rh(110) single crystals after high oxygen exposures (up to 10^{12} L) to ultrahigh vacuum.[17,18] However, high exposures at lower pressure may not generate the high-pressure phases because distinct p,T threshold conditions may exist beyond which certain phases become accessible based on the chemical potential of the phase (given that no kinetic limitations prevail). Theoretical modeling stressed the importance of subsurface oxygen incorporation as the critical step in the bulk oxidation of late transition metals, and calculations revealed that the critical oxygen coverage for incorporation into the subsurface region of Pd(111) (in tetrahedral sites) is close to the onset of bulk oxidation.[19,20] A recent combined in situ surface X-ray diffraction (SXRD) and DFT study has identified different crystalline phases of oxidized Pd(100) over an extended pressure and temperature range.[5] Here, we present photoemission spectroscopy (PES) measurements during the oxidation process of Pd(111) including subsurface

† Lawrence Berkeley National Laboratories, Chemical Sciences Division, University of California, Berkeley, CA 94720.

(1) Lundgren, E.; Kresse, G.; Klein, C.; Borg, M.; Andersen, J. N.; De Santis, M.; Gauthier, Y.; Konvicka, C.; Schmid, M.; Varga, P. *Phys. Rev. Lett.* **2002**, *88*, 246103.
(2) Gustafson, J.; Mikkelsen, A.; Borg, M.; Lundgren, E.; Köhler, L.; Kresse, G.; Schmid, M.; Varga, P.; Yuhara, L.; Torrelles, X.; Quiros, C.; Andersen, J. N. *Phys. Rev. Lett.* **2004**, *92*, 126102.
(3) Carlisle, C. I.; King, D. A.; Bocquet, M. L.; Cerda, J.; Sautet, P. *Phys. Rev. Lett.* **2000**, *84*, 3899; C. I. Carlisle, C. I.; Fujimoto, T.; Sim, W. S.; King, D. A. *Surf. Sci.* **2000**, *470*, 15.
(4) Over, H.; Kim, Y. D.; Seitsonen, A. P.; Wendt, S.; Lundgren, E.; Schmid, M.; Varga, P.; Morgante, A.; Ertl, G. *Science* **2000**, *287*, 1474.
(5) Lundgren, E.; Gustafson, J.; Mikkelsen, Andersen, J. N.; Stierle, A.; Dosch, H.; Todorova, M.; Rogal, J.; Reuter, K.; Scheffler, M. *Phys. Rev. Lett.* **2004**, *92*, 046101.
(6) Reuter, K.; Scheffler, M. *Appl. Phys. (NY)* **2004** *A78*, 793.
(7) Voogt, E. H.; Mens, A. J. M.; Gijzeman, O. L. J.; Geus, J. W. *Surf. Sci.* **1997**, *373*, 210.
(8) Legare, P.; Hilaire, L.; Maire, G.; Krill, G.; Amamou, A.; *Surf. Sci.* **1981**, *107*, 533.
(9) Weissman-Wenocur, D. L.; Shek, M. L.; Stefan, P. M.; Lindau, I.; Spencer, W. E. *Surf. Sci.* **1983**, *127*, 513.
(10) Zheng G.; Altman, E. I. *Surf. Sci.* **2000**, *462*, 151.
(11) Leisenberger, F. P.; Koller, G.; Sock, M.; Surnev, S.; Ramsey, M. G.; Netzer, F. P.; Kloetzer, B.; Hayek, K. *Surf. Sci.* **2000**, *445*, 380.
(12) Hartmann, N.; Krischer, K.; Imbihl, R. *J. Chem. Phys.* **1994**, *101*, 6717.
(13) Wolf, M. M.; Zhu, H.; Green, W. H.; Jackson, G. S. *Appl. Catal.* **2003**, *A244*, 323.
(14) Veser, G.; Wright, A.; Carreta, R. *Catal. Lett.* **1999**, *58*, 199.
(15) Taylor, K. C. *Catal. Rev. Sci. Eng.* **1993**, *35*, 457.
(16) Vesecky, S. M.; Rainer, D. R.; Goodman, D. W. *J. Vac. Sci. Technol.* **1996**, *A14*, 1457; Lyubovsky, M.; Pfefferle, L. *Catal. Today* **1999**, *47*, 29.
(17) Blume, R.; Niehus, H.; Conrad, H.; Böttcher, A.; Aballe, L.; Gregoratti, L.; Barinov, A.; Kiskinova, M. *J. Phys. Chem.* **2005**, *B109*, 14052.
(18) Dudin, P.; Barinov, A.; Gregoratti, L.; Kiskinova, M.; Esch. F.; Dri, C.; Africh, C.; Comelli, G. *J. Phys. Chem.* **2005**, *B109*, 13649.
(19) Todorova, M.; Li, W. X.; Ganduglia-Pirovano, M. V.; Stampfl, C.; Reuter, K.; Scheffler, M. *Phys. Rev. Lett.* **2002**, *89*, 096103.
(20) Todorova, M.; Reuter, K.; Scheffler, M. *Phys. Rev.* **2005**, *B71*, 195403.

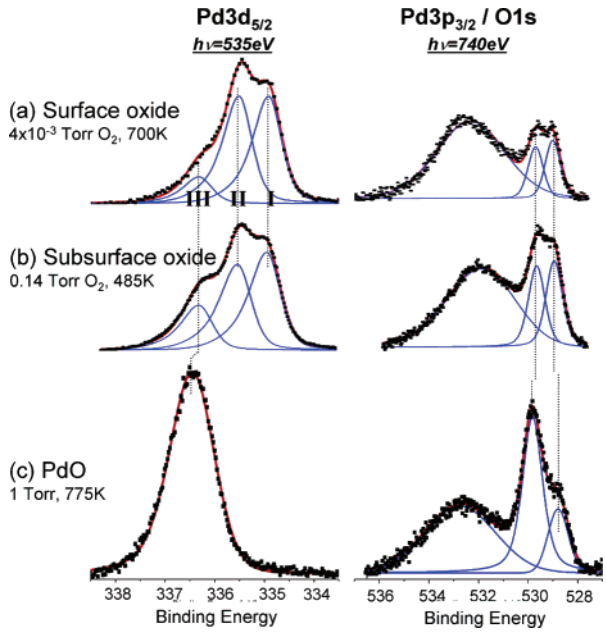

Figure 1. Pd3d$_{5/2}$ (left) and O1s/Pd3p$_{3/2}$ (right) XPS regions corresponding to different stages in the oxidation of Pd(111): (a) $\sqrt{6} \times \sqrt{6}$ surface oxide, (b) "subsurface oxide", and (c) bulk PdO. Peaks are normalized to the total Pd3d$_{5/2}$ and Pd3p$_{3/2}$ area, respectively. An extended version of this figure including the low-pressure phases and depth profiles can be found in the Supporting Information online.

incorporation and oxidation of the first few layers, and the kinetics of the different steps under oxygen pressures up to 1 Torr.

Experimental Section

The experiments were performed using a recently developed photoemission system that can operate at near-ambient pressures (i.e., up to several Torr), located at beamline 11.0.2 of the Advanced Light Source (ALS) of the Lawrence Berkeley National Laboratory in Berkeley, CA (a prototype of this system is described in Ref. 21). Photoelectrons from the sample are collected by a differentially pumped electrostatic lens system that refocuses the emitted electrons into the focal plane of a hemispherical electron energy analyzer.[22] We recorded the Pd3d ($h\nu = 535$ eV) and O1s ($h\nu = 740$ eV) spectra with the same electron kinetic energy in order to obtain the same information depth in all experiments ($\sim$0.6 nm,[23] corresponding to 2−3 layers of Pd-(111)). We also varied the photoelectron energy in order to obtain depth profiles of the O1s species for all structures and to check for final-state photoelectron diffraction effects. Modulations of the O1s and Pd3p peak intensities were observed for the surface oxide and "subsurface oxide" for kinetic energies below 250 eV due to final-state diffraction effects. The binding energy was calibrated with respect to the Fermi edge of the sample. The peaks were deconvoluted with asymmetric Gauss−Lorentz profiles after subtraction of a Shirley background and normalization by the corresponding energy-dependent X-ray photoionization cross sections.[24] No charging effects from the thin palladium oxide film were observed due to compensation by gas-phase ionization at pressures in the Torr range. After Ar sputtering and annealing at 1000 K in the preparation chamber the Pd(111) crystal was transferred to the ambient pressure chamber, where spectra were acquired at temperatures between 295 and 900 K and in the presence of oxygen at pressures from 10^{-6} Torr to 1 Torr.

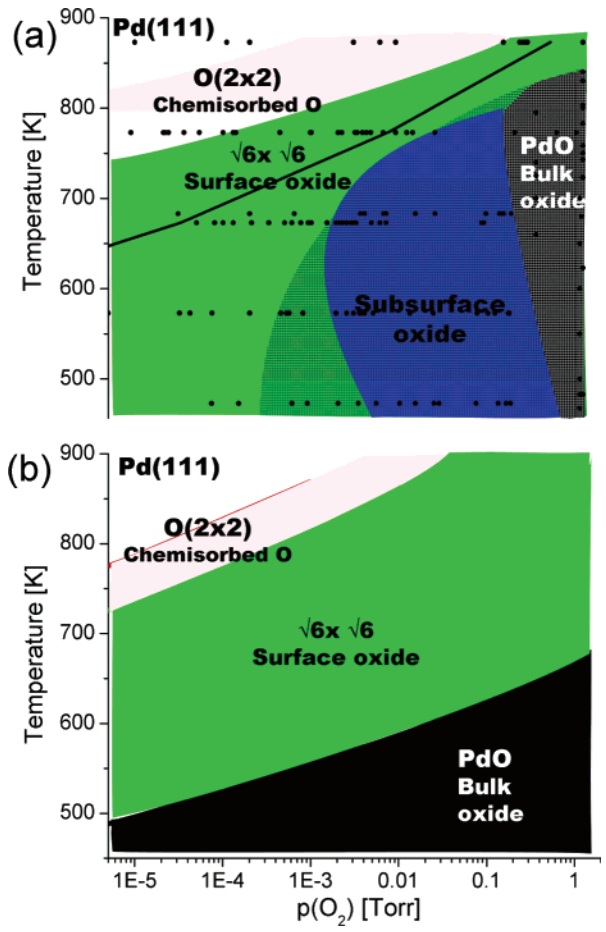

Figure 2. (a) Phase diagram showing the experimentally observed stability regions of the different palladium oxide structures as a function of p and T. The points mark the conditions under which XP spectra were acquired while increasing the oxygen pressure at fixed temperature (oxidizing conditions). At these points, no change was observed in the spectra over several minutes. The solid line indicates the phase transition of bulk Pd to bulk PdO as calculated by tabulated values of the enthalpies and heat capacities.[25] The hatched region shows the PdO bulk oxide stability region when the pressure is reduced from 1 Torr at fixed temperature. (b) Corresponding surface phase diagram, as calculated by transforming results from atomistic thermodynamics[6] into a p,T plot.

Results

Figure 1 shows spectra corresponding to the three phases and metastable structures that were observed during exposure of Pd-(111) to oxygen at pressures $>10^{-6}$ Torr. Each of them is characterized by peaks with unique binding energies and intensity ratios. Besides chemisorbed oxygen (not shown) and the $\sqrt{6} \times \sqrt{6}$ surface oxide (spectrum a) already reported in the literature[1], a new structure ("subsurface oxide") was found (spectrum b) followed by a bulk oxide phase (spectrum c), each in the specific pressure and temperature ranges that are shown in Figure 2. These structures were found to be stable over several minutes at a fixed temperature while increasing the oxygen pressure. When the pressure was decreased from 1 Torr at a fixed temperature, we observed differences in the stability, in particular an extended PdO stability region and no "subsurface oxide" (hatched region in Figure 2). We calculated the expected phase boundary for the formation of PdO by minimizing the

(21) Ogletree, D. F.; Bluhm, H.; Lebedev, G.; Fadley, C. S.; Hussain, Z.; Salmeron, M. *Rev. Sci. Instrum.* **2002**, *73*, 3872.
(22) SPECS Phoibos 150 hemispherical analyzer, Specs GmbH, Berlin, Germany.
(23) The information depth was calculated using the inelastic mean free path value for 200 eV electrons in Pd from Tanuma, S.; Powell C. J.; Penn, D. R. *Surf. Int. Anal.* **1997**, *17*, 911, under consideration of the detection angle of the electrons (40° to the surface normal).
(24) Yeh, J. J.; Lindau, I. *At. Data Nucl. Data Tables* **1985**, *32*, 1.

Gibbs Free Energy $\Delta G(p,T)$ using tabulated values for the enthalpies, entropies, and heat capacities[25] (dashed line in Figure 2). For $T > 650$ K, the phase boundary from surface to bulk oxide agrees very well with the Pd/PdO bulk phase boundary. In Figure 2b, we compare these data with the surface phase diagram obtained by atomistic thermodynamics. This diagram shows which phase would be most stable on the basis of the free energies from density-functional theory (DFT) calculations published in ref 6 as a function of p,T by using the oxygen chemical potential

$$\mu_{O2}(p,T) = kT\ln\left[\frac{p}{kT}\left(\frac{h}{\sqrt{2\pi MkT}}\right)^3 \frac{h^2}{\pi^2 L_{O2}{}^2 MkT}\right]$$

(with M: mass and L: bond length). The agreement with the experimental data is good for high temperatures and low pressures. For lower temperatures, obviously kinetics hinders the transition to the thermodynamically more stable bulk phases, as has been well described for Pd(100),[5] and the phase diagram does not reflect thermodynamic equilibrium. In particular, below the thermodynamic Pd/PdO phase boundary (solid line, Figure 2a), the surface oxide and "subsurface oxide" become metastable. Note that PdO in the presence of 1 Torr oxygen is stable up to higher temperatures (810 K) than theoretically predicted.

After chemisorbed oxygen has formed, the topmost surface layer oxidizes, forming a two-dimensional surface oxide[1] with a characteristic LEED pattern corresponding to a $\sqrt{6} \times \sqrt{6}$ superstructure for $p \geq 10^{-6}$ Torr and for temperatures below 750−900 K (see Figure 2). The surface oxide is characterized by $Pd3d_{5/2}$ peaks at 334.9 eV (I), 335.5 eV (II), and 336.3 eV (III) (Figure 1a), which have been attributed to Pd atoms with two (II) and four (III) O neighbors,[1] and bulk Pd (I).[19] The O1s region shows two peaks at 529.0 and 529.7 eV with an intensity ratio of ∼1, which have been assigned to two different oxygen species (3-fold and 4-fold coordinated O atoms)[1].

Two additional structures formed with increasing oxygen chemical potential (Figure 1). For oxygen pressures between 10^{-4} and 0.3 Torr and temperatures <650−750 K the surface oxide transforms into a new oxide structure with XPS peaks at identical binding energy positions as the surface oxide (Figure 1b) but with a Pd3p:O1s ratio changed from $PdO_{0.3}$ to $PdO_{0.6} \pm 0.1$ over the probed sample thickness (The O1s:Pd3d ratio at 200 eV is close to the averaged value obtained in the 120−250 eV energy range, and close to the value obtained by extrapolation from that measured at higher kinetic energies (300−600 eV)). The ratio between the $Pd3d_{5/2}$ peak areas at 336.3 and 335.5 eV has increased from 1:4 in the surface oxide to values between 1:2 and 1:1. Following the same assignment of coordination numbers as before the fraction of highly coordinated Pd atoms (four O neighbors) has increased. Peak positions are also unchanged in the O1s region, although the O intensity has increased. We will call this structure "subsurface oxide" in the following.

When the oxygen pressure is further increased into the Torr range PdO forms (Figure 1c). The $Pd3d_{5/2}$ region shows one single peak shifted by ∼1.6 eV compared to bulk metallic Pd. Previous studies reported Pd3d peak shifts between 1.1 and 1.9 eV for strongly oxidized Pd or PdO powders.[26−30] We find in our experiments that PdO is characterized by peak shifts ≥ 1.5 eV, smaller shifts being characteristic of the "subsurface oxide". While only one Pd species is observed in the Pd3d region, two different kinds of oxygen atoms are present with peaks at 529.8 and 528.9 eV, suggesting an oxygen-terminated surface. Photoelectron energy dependent measurements (depth profiling, Supporting Information available online) indicate that the lower binding energy peak originate closer to the surface than the higher binding energy peak.

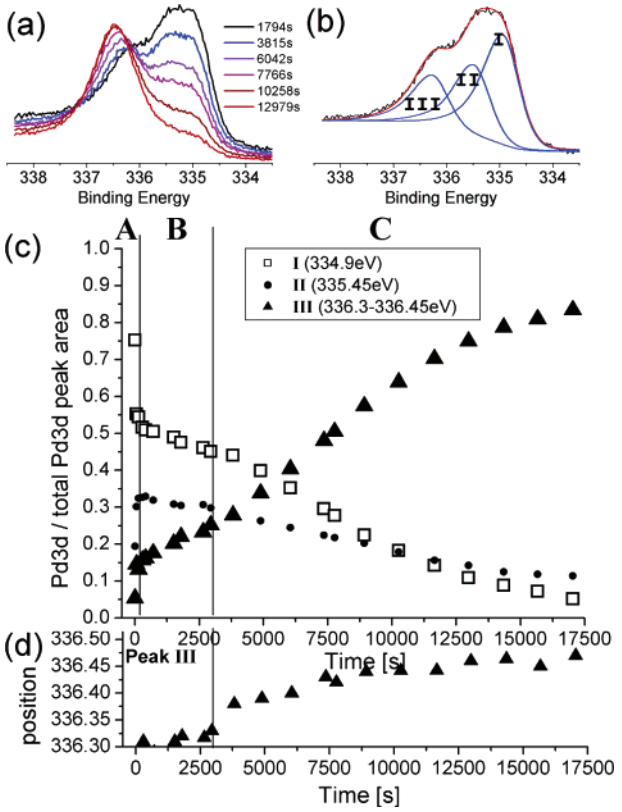

Figure 3. (a) Time evolution of the $Pd3d_{5/2}$ region during oxidation in 0.35 Torr O_2 at 660 K. (b) After deconvolution with the spectral characteristics of the different structures from Figure 1, the intensities of the various components (I−III) are obtained. (c) Plot of the intensities normalized to the total area as a function of time. Three different oxidation regimes (A−C) are observed that are discussed in the text. (d) Peak shift of peak III, indicating a chemical transformation in the initial stages of regime C.

The activation energies of formation for the various structures was obtained by acquiring photoemission spectra under constant p,T conditions as a function of time (Figure 3). The temporal evolution of the different $Pd3d_{5/2}$ peaks (I−III, Figure 3b) is plotted in Figure 3c. The oxidation process can be described by three steps that correspond to the regions labeled A−C in Figure 3c. First a surface oxide (A) forms (instantaneously in our time scale), as indicated by the rapid increase of peaks II and III. Subsequently, a slower process takes place (B), where the relative area of peak II decreases and that of peak III increases. This corresponds to the formation of the "subsurface oxide". When the peak II/III ratio reaches ∼1, oxidation

(25) Barin, I. *Thermochemical Data of Pure Substances*; VCH: Weinheim, 1992.
(26) Peuckert, M. *J. Phys. Chem.* **1985**, *89*, 2481.
(27) Banse, B.; Koel, B. E. *Surf. Sci.* **1990**, *232*, 275.
(28) Bondzie, V. A.; Kleban, P.; Dwyer, D. J. *Surf. Sci.* **1996**, *347*, 319.
(29) Voogt, E. H.; Mens, A. J. M.; Gijzeman, O. L. J.; Geus, J. W. *Surf. Sci.* **1996**, *350*, 21.
(30) Pillo, T.; Zimmermann, R.; Steiner, P.; Hufner, S. *J. Phys.: Condens. Matter* **1997**, *9*, 3987.

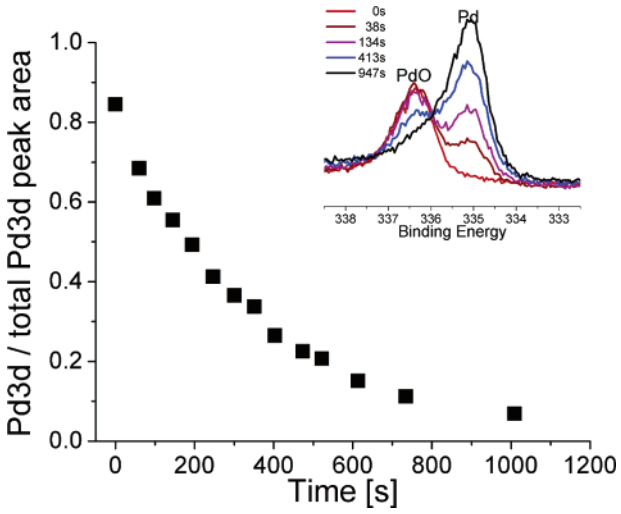

Figure 4. Time evolution of the $Pd3d_{5/2}$ region during reduction in 3×10^{-3} Torr O_2 at 775 K: Ratio of the integrated intensity of the deconvoluted PdO peak to the total Pd3d signal intensity. The inset shows a sequence of $Pd3d_{5/2}$ spectra recorded in the presence of 3×10^{-3} Torr O_2 at 775 K.

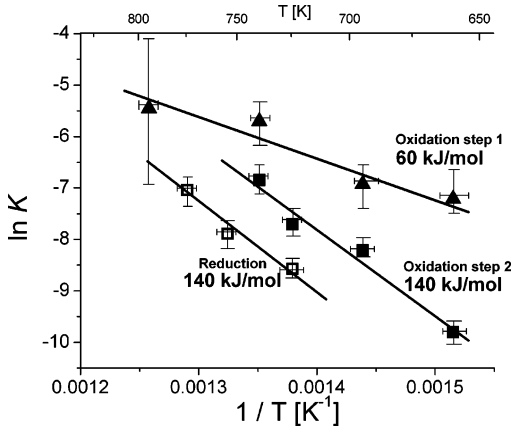

Figure 5. Arrhenius plot of the initial oxidation rate versus $1/T$. The slope of the best line fits gives the activation energy for the transformation from surface to "subsurface oxide" (filled triangles), from "subsurface oxide" to PdO (filled filled squares), both in 0.35 Torr O_2, and for the reduction of PdO to Pd(111) in 3×10^{-3} Torr O_2.

accelerates and bulk PdO is formed. At this point, the O:Pd ratio also increases.

The time dependent reduction process was also followed by monitoring the XPS signals after rapidly reducing the O_2 pressure and increasing the temperature. A typical time trace is shown in Figure 4. The PdO related Pd3d peak at 336.4 eV decreased while the metal related peak increased and shifted from 335.2 eV to 334.9 eV during reduction.

To determine the activation energies for the reduction and the two oxidation steps, time traces similar to those in Figures 3 and 4 were obtained for temperatures between 660 K and 795 K. The oxygen pressures were 0.35 ± 0.03 Torr for oxidation and 3×10^{-3} Torr for reduction. From a semilogarithmic plot of the initial oxidation rate versus $1/T$, the activation energy E_a for the formation of the "subsurface oxide" was estimated to be ~60 kJ/mol (Figure 5). The second oxidation step, corresponding to the transformation to bulk PdO requires an activation energy of ~140 kJ/mol. The same value was estimated for the activation energy of reduction, in agreement with the value obtained from ellipsometry measurements.[7]

Discussion

The time traces in Figures 3 and 4 were fitted to different apparent reaction orders, and the best fit was obtained for a first-order rate law. It is straightforward to compare our observations of oxide growth with thin film oxidation models based on the Cabrera−Mott and Fehlner−Mott models.[31,32] These theories describe thin film oxidation by cation (Cabrera−Mott) or anion (Fehlner−Mott) diffusion through the oxide film, driven by the electric field between the negatively charged surface oxide layer and the bulk metal reservoir. For this purpose, the y-scale of the time traces has to be transformed from I/I_{total} to the thickness d of the growing film. Assuming a homogeneous film composition, we estimated the film thickness by a simple function $d = \lambda * \exp(-I/I_0)$ (with λ: electron escape width for the selected energy, I:Pd3d(PdO) intensity, I_0:Pd3d-(PdO) intensity for a completely oxidized film (within the probed depth)). Our data could be fitted with an inverse logarithmic rate law suggesting cation diffusion in a Cabrera−Mott type mechanism. However, due to the reduced number of data points and the limited information depth of 0.6 nm other thin film oxidation models could not be completely ruled out.

The main difference between the surface oxide and the "subsurface oxide" concerns the peak intensities. In particular, the depth profiles of the O1s peaks (Supporting Information online) show that the two oxygen species are no longer confined to the surface region. Note, however, that the higher binding energy O1s species of the surface oxide has quite some intensity at higher kinetic energies, implying that also the surface oxide is not confined to the topmost layer as previously proposed.[1]

No LEED pattern could be obtained for the "subsurface oxide" because of charging effects of the insulating film, but XPS intensity variations at low kinetic energies due to photoelectron diffraction reveal that the "subsurface oxide" was crystalline. Since neither the O1s nor the Pd3d peaks of the subsurface oxide are shifted with respect to the surface oxide, the chemical nature of both structures appears to be similar. This implies that the surface oxide is no longer confined to the topmost surface layer, but can also grow into the subsurface region while maintaining an epitaxial relationship to the underlying Pd(111). Epitaxial growth of the "subsurface oxide" would not require a large restructuring of the film, which is consistent with the lower activation energy found experimentally. Transformation into bulk PdO, which is the stable phase,[6] requires a higher activation energy and for that reason the "subsurface oxide" is metastable. This conclusion is supported by the observation that the "subsurface oxide" does not form during reduction of PdO, which proceeds directly from bulk to surface oxide. However, in addition to the lower activation energy, the initial oxidation rate for the "subsurface oxide" is faster than that of PdO (higher rate constant K and thus less negative ln$K$ for all T, Figure 4), therefore the "subsurface oxide" can be observed over an extended pressure and temperature range (Figure 2). The phase transition to bulk PdO involves a structural transformation that is reflected by the shift of 0.15 eV of the Pd3d peak III during the initial stages of bulk oxidation (Figure 3d, regime C).

The growth of metastable epitaxial oxides might be a general phenomenon in the oxidation of metals. As the surface free

(31) Cabrera, N.; Mott, N. F. *Rep. Prog. Phys.* **1948−49**, *12*, 163.
(32) Fehlner, F. P.; Mott, N. F. *Oxid. Met.* **1970**, *2*, 59.

energy of oxides is lower than that of metals in most cases, oxides are expected to wet the metal surface, assuming that the interface free energy is negligible.[33] In most cases, wetting is energetically not favored due to the lattice mismatch between the oxide layer and the metal. However the low-index surfaces of late transition metals, such as Ag, Ni, Pd, Rh, and Ru,[1−5] form two-dimensional, epitaxial surface oxides. Recent in situ SXRD studies showed no evidence for subsurface growth of the epitaxial surface oxide on Pd(100) and Rh(111).[2,5] Theory has shown that the ability to incorporate oxygen into the subsurface region depends on the lattice deformation cost and decreases from Ru to Ag,[19] and as the stability range of the surface oxide is larger to the right of the periodic table,[2] an oxidation mechanism as observed in this study is more likely for (but not restricted to) Ag where indeed such a growth mechanism has been theoretically predicted.[34] The energy balance between the free energies, in particular, the energy gain due to the enthalpy of oxide formation vs the energy cost due to lattice deformation and interfacial strain will determine when an epitaxial subsurface oxide growth mode is accessible.

The reduction of PdO occurred at significantly lower pressures than the oxidation and, for $T > 650$ K, is close to the calculated phase boundary (Figure 2). The oxidation−reduction hysteresis thus basically covers the "subsurface oxide" stability region. While oxidation proceeds by the easy formation of a metastable "subsurface oxide", reduction goes directly from bulk PdO to Pd(111). The reduction time traces agree well with those reported previously, and are consistent with a diffusion-controlled reduction model.[14] The initial binding energy shift to 335.2 eV in our experiments may indicate the presence of chemisorbed oxygen, and/or some bulk dissolved oxygen (335.2 eV[11]) during reduction to metallic Pd(111) (334.9 eV[11]). No peaks between 335.2 and 336.3 eV were observed during the transformation, thus the "subsurface oxide" is not an intermediate during reduction.

(33) Bauer, E. *Z. Kristallogr.* **1958**, *110*, 372; **1958**, *110*, 395.
(34) Li, W.-X.; Stampfl, C.; Scheffler, M. *Phys. Rev.* **2003**, *B67*, 045408.

Conclusions

Using ambient pressure photoemission, we have studied the kinetics and the surface and subsurface structures formed during the oxidation of Pd(111). After chemisorption, oxidation proceeds in three steps via a surface oxide that first grows into the bulk before restructuring to the energetically favored bulk PdO. No "subsurface oxide" is observed during diffusion-controlled reduction. We propose that an epitaxial "subsurface oxide" forms as a metastable intermediate in the bulk oxidation, and that the low activation energy for this process kinetically stabilizes the "subsurface oxide". This explains the observed reduction/oxidation hysteresis. The proposed mechanism may apply to the oxidation/reduction of other late transition metals as well.

Acknowledgment. This work was supported by the Director, Office of Energy Research, Office of Basic Energy Sciences, Chemical Sciences Division and Materials Sciences Division of the U.S. Department of Energy, under Contract No. DE-AC03-76SF00098. GK thanks the Alexander-von-Humboldt foundation for financial support.

Supporting Information Available: Deconvoluted $Pd3d_{5/2}$ and $O1s/Pd3p_{3/2}$ core level spectra and the corresponding normalized O1s:Pd3p core level-intensity-ratio (open symbols) as a function of kinetic energy of the emitted photoelectrons (depth profile) of clean Pd(111), chemisorbed $O(2 \times 2)$/Pd-(111), the $\sqrt{6} \times \sqrt{6}$ surface oxide ("Pd_5O_4"), the "subsurface oxide", and bulk PdO (FIGURE). The filled symbols show the O1s:Pd3p intensity ratio of the higher binding energy O1s component (around 529.7 eV, filled circles) and the lower binding energy O1s component (around 529.0−528.8 eV, filled squares). This material is available free of charge via the Internet at http://pubs.acs.org.

JA055754Y